ELSEVIER

Catalysis Today 26 (1995) 23–32

CATALYSIS TODAY

On the vital roles of zeolitic matrix in catalysts for deNO$_x$ reactions under conditions similar to diesel engine exhaust

Tomoyuki Inui *, Shinji Iwamoto, Katsuhiko Matsuba, Yuichi Tanaka, Takashi Yoshida

Division of Energy and Hydrocarbon Chemistry, Graduate School of Engineering, Kyoto University, Sakyo-ku, Kyoto 606-01, Japan

Abstract

The physical and chemical properties of a Cu-ion-exchanged Al-silicate with an MFI or A structure and Cu-containing silicate, in which Cu was incorporated into MFI or A structure were compared. It was found that the stability and catalytic performance of Cu-containing silicates were superior to those of Cu-ion exchanged Al-silicates. Furthermore, the advantageous factors of zeolite materials for deNO$_x$ reaction were investigated by simulating the acid properties and the thermal stability of the framework. Such metal-containing silicate catalysts have large potentials as the deNO$_x$ catalysts for diesel engine exhaust. The reaction characteristic was explained by the microscopic sequential reaction (MSR) mechanism.

1. Introduction

Recently, catalytic conversion of NO in the presence of excess O_2 and a low concentration of hydrocarbon has been intensively studied to decrease the NO_x in the exhaust gas from diesel engines and lean-burn facilities to a harmless level. A variety of catalysts, such as alumina [1,2], other metal-oxides [3,4], and microporous crystalline catalysts [5–9] have been studied. Above all, microporous crystalline catalysts, such as zeolites and their related materials are more suitable for the practical application especially at high space velocity conditions [10–12]. Many types of ion-exchanged zeolites were investigated as catalysts for the deNO$_x$ reaction. However, these catalysts have limitations owing to the properties of their mother zeolites such as thermal stability, acidic property and ion exchange capacity. On the other hand, metallosilicates, which were synthesized by the rapid crystallization method adding the other elements in the reaction gel in the hydrothermal stage, have quite large potentials for precise modification of the catalytic properties [13,14]. In fact, many promising results were already reported using MFI-type metallosilicates [15,16] and others [17,18]. The validity of metallosilicates for the deNO$_x$ reaction was also shown using MFI-type Co-containing silicates [19,20]. Those properties were attributed to the high and stable distribution of the incorporated elements. However, the significance of metallosilicate structures for the objective reaction seems to be still not yet understood. Therefore, in this paper, we compared the physical and chemical properties and catalytic performance of ion-exchanged zeolites and metallosilicates and discussed their correlation in detail. Furthermore, computer simulation was applied to investigate

* Corresponding author.

SSDI 0920-5861(95)00096-8

the advantageous factors of metallosilicates, such as strength and distribution of acidity and thermal stability, for the objective reaction.

2. Experimental

2.1. Catalyst preparation

Cu-containing zeolite A (Cu–A) was synthesized applying the concept of the rapid crystallization method [13,14]. An example of the procedure is as follows: 5.30 g of $Cu(NO_3)_2 \cdot 3H_2O$, 7.65 g of $NaAlO_2$, 12.00 g NaOH, and 9.10 g of No. 3 brand water glass were dissolved into 20, 25, 25, and 100 ml of distilled water, respectively. The $Cu(NO_3)_2 \cdot 3H_2O$ solution was added to the water glass solution dropwise while vigorous stirring using an ultra disperser in an ice bath. $NaAlO_2$ solution was mixed with NaOH solution and added to the above mentioned solution. After the gel became uniform, it was further milled by a motor-driven mortar. Then this mixture was transferred to a closed glass bottle, and heated at 85°C for 6 h. The obtained solid materials were washed with distilled water until the pH of the washing water became 7, followed by drying overnight at 110°C. Finally, the crystals were calcined at 400°C for 2 h in an air flow. Loading of 0.1 wt.-% Rh on Cu–A was made by an ion exchange method using $Rh(NO_3)_3$. Copper supported on γ-Al_2O_3 was prepared by an ordinary impregnation method. Cu-silicate and Al-silicate were prepared by the rapid crystallization method [13,14]. Cu-ion exchanged A-type zeolite (Cu/A) and MFI-type zeolites (Cu/Al-silicate) were prepared by a usual ion-exchange method with a 1 N $Cu(CH_3COO)_2$ aqueous solution at room temperature.

2.2. Characterization

A TG-DTA Shimadzu Thermal analyzer DT-30 was used to measure the redox response and the temperature programmed reduction (TPR). For the measurement of the redox response, a 20 mg portion of the sample was placed in a sample pan and a flow N_2 gas containing 4% O_2 or H_2 was allowed to flow with a feed rate of 40 ml/min. The amount of O_2 or H_2 supplied was sufficient to oxidize or to reduce the sample. On the other hand, for TPR measurement, the sample was first heated in 4% O_2–96% N_2 from room temperature to 600°C with a constant heating rate of 10°C/min and maintained at that temperature for 30 min. After it cooled down, it was heated again in 4% H_2–96% N_2 with the same heating rate.

2.3. Catalytic reaction

The catalytic reaction test was carried out by using an ordinary flow apparatus. The catalyst in powder form was tabulated and crushed into a 15–24 mesh to provide for the reaction. A 0.5 g (ca. 0.7 ml) portion of the catalyst was packed in a quartz tubular reactor of 8 mm inner diameter. After drying in a helium flow at 400°C for 30 min, a reaction gas was introduced in a temperature range from 200 to 500°C with an SV 2500 h^{-1}. The reaction gases and products were analyzed by using a gas chromatograph (Shimazdu GC-4C PT, MS-5A column) equipped with an integrator. Oxygenated products were analyzed precisely by using GC-MASS spectroscopy (Shimazdu GCMS-QP 1000EX).

2.4. Computer calculation of the characteristic behavior of various matallosilicates

The acidic properties of MFI-type and BEA-type metallosilicates were simulated by the Monte Carlo method. The potential energies of the NH_3 molecules in the metallosilicates were calculated by using a DREIDING II force field developed by Goddard III [21,22]. In this force field the interactions (E) consist of bond stretch (E_B, two body), bond-angle bend (E_A, three-body), dihedral angle torsion (E_T, four-body), inversion (E_I, four-body), van der Waals (E_{vdw}), electrostatic (E_Q), and hydrogen bond (E_{hb}) terms, as in the following equation:

$$E = E_B + E_A + E_T + E_I + E_{vdw} + E_Q + E_{hb} \quad (1)$$

The fixed pressure (grand canonical) algorithm [23] used in these simulations was as follows: (i) Creation of a molecule; an ammonia molecule is placed at a random position in the domain of the metallosilicate framework, and weather its configuration is accepted or not is judged according to the energy change, i.e., with the probability P expressed in the following equation:

$$P = \min[1, \exp\{-DU/kT - \ln\{(N+1)\}kT/pV\}] \quad (2)$$

where DU is the configurational energy change, N is the current number of molecules in the framework of metallosilicate, p is the pressure of molecules in the gas phase, and V is the cell volume. (ii) Removal of a molecule; a random ammonia molecule located in the framework is chosen, and new configuration will be accepted with the following probability:

$$P = \min[1, \exp\{-DU/kT + \ln(NkT/pV)\}] \quad (3)$$

(iii) Translation of a molecule; we choose a random molecule in the framework and translated it by random amount within a cube of size 2d ($d = 1$ Å), and will accept new configuration with probability P:

$$P = \min[1, \exp\{-DU/kT\}] \quad (4)$$

(iv) Rotation of a molecule; a random molecule and a random axis are chosen in the framework, and the molecule is rotated by a random amount within the range $-d$ to $+d$ ($d = 50$ degrees). New configuration will be accepted based on the energy change as for Eq. (4). The amount of adsorbed were counted after this cycle and these cycles were repeated 100 000 times.

The thermal stabilities of MFI, MOR, and BEA-type Al-silicates were calculated by the MD method using DREIDING II force field mentioned above in the temperature range from 300 to 1300 K under a pressure of 1 atm. The charges of the atoms were determined by considering electronegativities. All the samples were treated as H-type zeolites with Si/Al atomic ratio = 31, 31, and 11 for MFI, BEA, and MOR, respectively.

3. Results and discussion

3.1. Comparison of the catalytic property of Cu-ion-exchanged Al-silicate and Cu-incorporated MFI-type silicate

Cu/Al-silicate and Cu-silicate gave XRD patterns similar to those of the MFI structure, and no indication for the presence of isolated copper oxides. BET surface area of Cu-silicate was 373 m^2/g and it was almost the same as that of Cu/Al-silicate (380 m^2/g). However, the effective diffusion coefficient β of Cu-silicate, 2.55, was much larger than that of the Cu/Al-silicate [24], indicating that the space in the pore of Cu-silicate is more vacant due to incorporation of Cu in the framework. Steady activities of NO decomposition under O_2-absent condition on those catalysts were ca. 80% and 22% after 8 h on stream, respectively. The integrated moles of converted NO were much larger than Cu atoms in both catalysts. These results were clearly different from the result of the catalyst prepared by a coprecipitation method [24], and indicate that NO was decomposed catalytically. It seems to be an advantage to Cu/Al-silicate that larger amounts of copper were incorporated in it and showed higher activity for the NO decomposition reaction in the absence of oxygen than those of Cu-silicate [24–27]. However, the position of copper in the Cu/Al-silicate is not in the framework but in the cation-exchange sites. Redox properties of both catalysts are shown in Fig. 1. The redox responses of H-Cu-silicate are about one third of those of Cu/H-Al-silicate, which is consistent with the difference of the NO conversion of both catalysts. This kind of copper would be unstable and have a fatal disadvantage because of sintering or evaporation which happens easily when exposed to high temperatures under redox-cycle conditions [28]. In order to confirm the differences in stability of both catalysts, the CO oxidation test by the forced-oscillating reac-

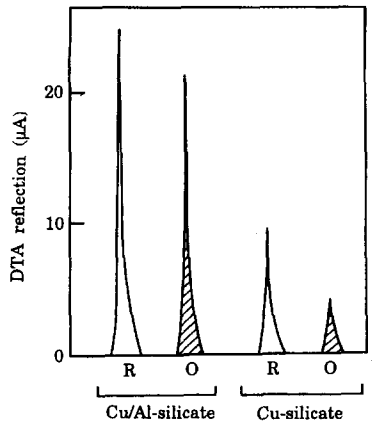

Fig. 1. Redox response measured by DTA for Cu-ion exchanged Al-silicate and H-Cu-silicate at 250°C. R: H_2 reduction; O: O_2 oxidation.

tion method [29] was conducted. By this method, the redox processes of catalyst surface during the reaction can be realized; therefore, through examining the redox response repeatedly, the stability of catalyst can be evaluated. As a result, the redox cycles of Cu-silicate by temperature-elevation and lowering with a constant rate were shown to be reproducible, indicating that the copper parts were stable against redox cycles. On the other hand, as for Cu/Al-silicate the width of the hysteresis narrowed with repeating redox cycles. Furthermore, the curvatures of CO conversions were much sharper using Cu-silicate compared with Cu/Al-silicate during increases and decreases in temperature. This indicates that the copper was sintered gradually on Cu/Al-silicate. The comparison mentioned above is summarized in Table 1.

3.2. *Characteristics of Cu-containing zeolites*

Since the stability of the intermediate oxidation-state of copper is supposed to be one of the key points in realizing the NO decomposition [30–32], TPR responses for various catalysts were compared (Fig. 2). The Cu-ion-exchanged A-type zeolite (Cu/A) showed one peak at around 270°C, having a shoulder at 240°C. In the case of the Cu/A it was somewhat difficult to reduce compared with Cu–A, and the reduction shifted to a higher temperature; however, once reduction began it progressed successively from CuO to Cu without showing a stable intermediate state. These properties reflect that in the case of the ion-exchanged method, copper forms considerably larger clusters, or copper particles block the part of pore channels, and retard the diffusion of hydrogen and water formed, resulting in the delay of hydrogen reduction. As for the Rh/Cu–A catalyst, the Rh parts scattered on the surface of the catalyst and accelerated the reduction of the copper oxides [33]. However, single peak was consistently observed. On the other hand, the Cu-incorporated A-type zeolite (Cu–A) showed two distinct peaks appearing at 160 and 250°C. The higher temperature peak was near the single peak of Cu/A, however, the lower one was far from the shoulder peak. The weight decreases corresponded to the changes of CuO to Cu_2O and Cu_2O to Cu, respectively. This observation is consisted with the results observed by Tanabe and Matsumoto [34]. These facts indicate that only the structure of Cu dispersion, which was made in the course of crystallization, can afford the stable intermediate oxidation state.

3.3. *Effect of hydrocarbon addition on NO conversion under an excess oxygen condition*

In the previous study on the reduction of the pre-oxidized supported copper oxides using various kinds of reductants, it was found that the reduction rates of the reductants were in the following order: $CO > H_2 > CH_4 > C_3H_8$ [32]. This order was the same as that obtained in the rate of O_2 adsorption on the surfaces reduced with these reductants and means that the oxidation states of the reduced surfaces are changeable with the kind of reductants suggesting the importance of the microscopic change of the surface.

Furthermore, through the study on catalytic combustion rates of C_1–C_{14} straight chain saturated hydrocarbons on a supported Pt–CeO_2 catalyst [35], it was found that the combustion rates of hydrocarbons were maximal at around carbon number C_7–C_{10}, and that above C_8 hydrocarbons the combustion rates gradually decreased with the increase in carbon number owing to the incom-

Table 1
Comparison of characteristics between Cu-ion-exchanged H-ZSM-5 and Cu-metallosilicate having an MFI structure

	Ion-exchanged	Incorporated into framework
Maximum Cu content	200% of H^+ (considerably large)	Ca. 0.6 wt.-% (fairly small)
Redox response	Steady (largely amplified)	Increased gradually (small amplified)
NO decomposition activity		
Non-O_2 condition	Fairly large	Medium
Excess O_2 condition	None	None
Stability		
(Combustion test-forced oscillating reaction method)	Weak	Strong

plete combustion. It was also found that the hysteresis in the forced oscillating reaction test were very different as for each hydrocarbon added. It is considered that the hydrocarbons added should be distributed as widely as possible in the catalyst bed to be used for NO decomposition reaction effectively before they are consumed by the combustion. The other reductants such as hydrogen and carbon monoxide, which combust too easily, give little effect on the objective reaction because these reductants are consumed just at the entrance of the catalyst bed.

According to this consideration, the NO decomposition in the presence of excess O_2 on Cu–A was studied with an addition of saturated C_1, C_2, and n-C_7 hydrocarbons (Fig. 3). The temperature dependencies of NO conversion reactions were consistent with the combustion rates of hydrocarbons added [27].

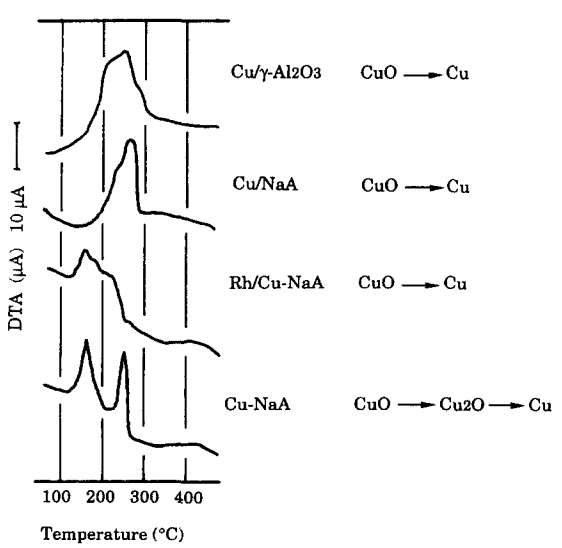

Fig. 2. Temperature programmed reduction (TPR) profiles for various Cu-containing catalysts.

From these results, it was expected that when a proper kind of hydrocarbon was chosen, the reduction of the oxidized catalyst surface was attained properly and the NO decomposition reaction progressed smoothly. Addition of higher hydrocarbons such as n-C_8, n-C_{10}, and n-C_{16} saturated hydrocarbons were examined in a more oxidative condition. The amount of added hydrocarbon was set at about 0.6 molar ratio of complete combustion stoichiometry. As shown in Fig. 4, the magnitude of NO conversion was in the following order: n-C_{16} > n-C_{10} > n-C_8, and around 300–350°C each NO conversion attained its maximum. Especially, in the case of cetane (n-C_{16}) addition, the complete NO conversion was achieved in this temperature range, and even above 350°C, the decrease of NO conversion at higher temperature range was very gentle com-

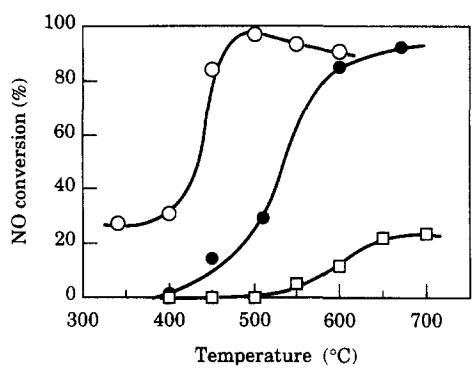

Fig. 3. Effect of light hydrocarbons added in the reaction gas with fairly low oxygen concentration on NO conversion. Cat: Cu–A, SV = 2500 h^{-1}. □: NO 2.0%, O_2 3.1%, CH_4 4.8% (O_2 excess ratio 0.43); ●: NO 2.3%, O_2 2.8%, C_2H_6 2.4% (O_2 excess ratio 0.47); ○: NO 1.6%, O_2 3.0%, n-C_7H_{16} 0.85% (0_2 excess ratio 0.41).

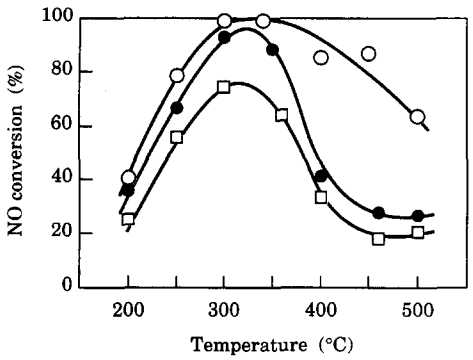

Fig. 4. Effect of long chain hydrocarbons added in the reaction gas under an excess oxygen condition on NO conversion. Cat: Cu–A, NO 9600 ppm, O_2 11.0%, SV 2500 h^{-1}. □: n-C_8H_{18} 6500 ppm; ■: n-$C_{10}H_{22}$ 4100 ppm; ○: n-$C_{16}H_{34}$ 2600 ppm.

pared with other cases. As shown in Fig. 5, the conversions of hydrocarbons to CO_2 and CO during the NO conversion were observed above ca. 200°C and these increased exponentially up to ca. 300°C, and above that temperature the increase suddenly slowed down. It is noteworthy that the order of NO conversion was the inverse of the order of hydrocarbon conversion as to the kind of hydrocarbons added to the reaction gas. As shown in Fig. 6, when NO was not involved in the reaction gas, the conversion of each hydrocarbon increased exponentially with the increase in the reaction temperature, and reached 100% conversion level until 300–350°C; above that temperature, the complete conversion was maintained, this is different from the case of conversion in the presence of NO.

As can be understood from the comparison between Fig. 4 and Fig. 5, the increase of NO conversion up to 300°C was markedly larger than the increase of hydrocarbon conversion, although the temperature range for the increase of both conversions coincided. This suggests that NO conversion progresses effectively with less amount of hydrocarbon reacting on a considerably small number of active sites. The decrease in NO conversion at higher temperature must be attributed to the fact that the catalyst surface is more oxidized, creating a condition which is not suitable for NO decomposition.

In the case of the addition of cetane, small amounts of partial oxidation products such as aldehydes, 2-ketones, α-alkylfuranes, etc., were detected [27]. It is considered that these products strongly adsorbed on the catalyst surface, and retarded a deep oxidation of the catalyst surface; consequently, the decrease of the NO conversion would be moderate even at the higher temperature range.

Since a very small amount of hydrocarbons was shown to be effective for the NO conversion, we tried to reduce the concentration of cetane added in the NO conversion reaction, and the results are shown in Fig. 7. The molar ratios of cetane added to the complete combustion stoichiometry were 0.56, 0.15, 0.04 for the concentration of cetane 2600, 700, and 190 ppm, respectively. The degree of decrease in NO conversion was very small, considering the decrease of the combustion stoi-

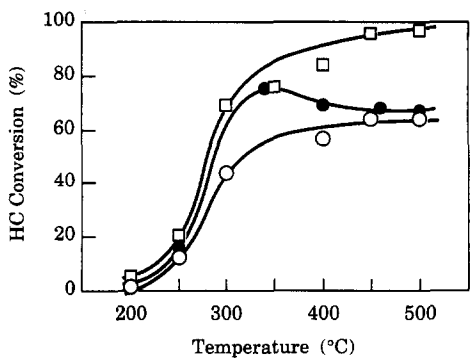

Fig. 5. Effect of temperature on hydrocarbon combustion during NO conversion reaction shown in Fig. 4. Cat: Cu–A, NO 9600 ppm, O_2 11.0%, SV 2500 h^{-1}. □: n-C_8H_{18} 6500 ppm; ●: n-$C_{10}H_{22}$ 4100 ppm; ○: n-$C_{16}H_{34}$ 2600 ppm.

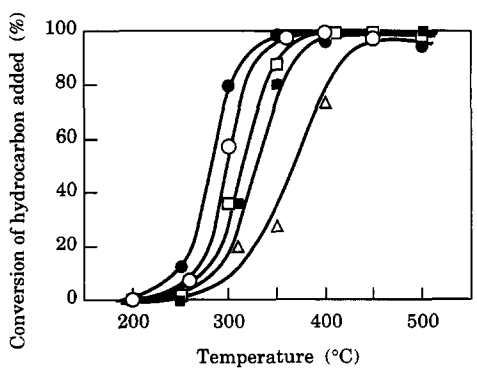

Fig. 6. Effect of temperature on catalytic combustion of various hydrocarbons in NO conversion reaction. Cat: Cu–A, NO 9600 ppm, O_2 11.0%, SV 2500 h^{-1}. △: n-C_6H_{14} 0.70%; ■: n-C_7H_{16} 0.78%; □: n-C_8H_{18} 0.46%; ●: n-$C_{10}H_{22}$ 0.48%; ○: n-$C_{16}H_{34}$ 0.34%.

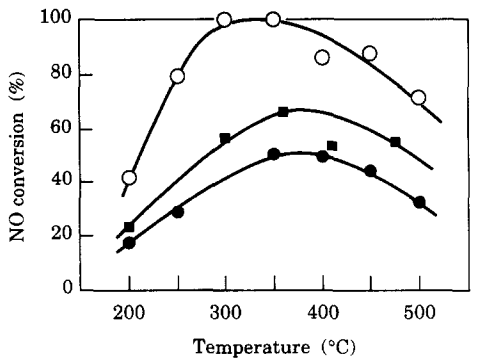

Fig. 7. Effect of cetane concentration on NO conversion. Cat: Cu–A, NO 9600 ppm, O_2 11.0%, SV 2500 h^{-1}, n-$C_{16}H_{34}$. □: 2600 ppm; ●: 700 ppm; ○: 190 ppm.

chiometry, and even with the addition of 190 ppm cetane, 50% NO conversion was still realized.

3.4. Consideration on the reaction mechanism

To explain the whole experimental results of the redox properties and the NO decomposition in the presence of excess oxygen with the catalytic combustion of a very small amount of hydrocarbon having a considerably large carbon number, successive occurrence of the consecutive reactions shown in (5-1), (5-2) and (6-1), (6-2), and parallel reactions (6-3) and (7) were considered.

$$C_xH_y + nO_{ad}[S] \xrightarrow{k_1} C_xH_{yad}(nO_{ad}[S]) \quad (5\text{-}1)$$

$$C_xH_{yad}(nO_{ad}[S]) + mO_{ad}[S] \xrightarrow{k_2} xCO_2 + (y/2)H_2O + (2x+y/2)[S] + [(n+m)-(2x+y/2)]O_{ad}[S] \quad (5\text{-}2)$$

$$NO + [S] \underset{k_4}{\overset{k_3}{\rightleftharpoons}} NO_{ad}[S] \quad (6\text{-}1)$$

$$2NO_{ad}[S] \xrightarrow{k_5} N_2 + O_2 + 2[S] \quad (6\text{-}2)$$

$$2NO_{ad}[S] \xrightarrow{k_6} N_2 + 2O_{ad}[S] \quad (6\text{-}3)$$

$$O_2 + 2[S] \xrightarrow{k_7} 2O_{ad}[S] \quad (7)$$

A proper hydrocarbon adsorbing on the oxygen-adsorbed catalyst surface is combusted by consuming the oxygen on the surface explosively. Successively, the combustion products, CO_2 and H_2O, desorb and the active sites for NO decomposition appear. These active sites would be oxidized by the oxygen; however, NO is adsorbed and decomposed on the active sites at proper temperature. This reaction mechanism is based on the understanding of the non-linear phenomena like the oscillating reaction on the solid catalyst surface [31]. Therefore, we have propose to call this mechanism Microscopic Sequential Reaction mechanism (MSR mechanism) [19,24,27,36]. The following points are thought as important factors to run the reaction mechanism smoothly:

(1) metal oxides, which are oxidized and reduced considerably easily, are highly dispersed and stably anchored on the matrix of microporous crystallines with a crystallographical regularity. In other words, catalytically active metal or metal oxide species are isolated with proper distance on the matrix of microporous crystals and consequently, this situation easily make possible the localized reduction and oxidation phenomena due to catalytic combustion of the very diluted combustible hydrocarbon added in the reaction gas;

(2) the reaction rates of NO decomposition and combustion of hydrocarbons added are comparable at around 300–400°C;

(3) straight chain hydrocarbons are preferred for the hydrocarbon to be added in the reaction gas, because bulky hydrocarbons such as cyclohexane and iso-octane showed a little effect on the NO reduction compared with n-hexane and n-octane, respectively, owing to their low diffusivities in the pore channels [37].

In the light of this new mechanism it is expected that many other new catalysts will be developed.

3.5. Simulation of NH_3 adsorption and thermal stability of various metallosilicates

The geometric distribution of NH_3 molecules on MFI-type metallosilicates and BEA-type metallosilicates was investigated, respectively [38]. In each case the adsorbed NH_3 molecules were close to the protons, which are accompanied

by the substituted metal elements. The amounts of the NH_3 adsorbed are summarized in Table 2. The order of the acid property was: Al > Ga ≫ Fe, for each MFI and BEA type metallosilicates expressed with the kind of metal, and MFI-type metallosilicates have higher acid strength than those of BEA-type. This difference was attributed to the fact that in the case of BEA-metallosilicates NH_3 could adsorb only in close position to protons while NH_3 was adsorbed widely in the pore for MFI-metallosilicates. These simulation results consistently corresponded to the experimental results, such as NH_3-TPD or hydrocarbon conversions [14,15,39]. This examination was expanded for other molecules and types of metallosilicates and demonstrated the high validity of this method.

The thermal stability of the various zeolites was estimated by changing the Si/Al ratio in the framework [40]. Fig. 8 shows the change of the potential energy within 2.0 ps at 1300 K for H-Al-MFI (Si/Al=31), H-Al-BEA (Si/Al=31), and H-Al-MOR (Si/Al=11) silicates. As for H-Al-MOR the calculation was not completed suggesting the collapse of the framework. As for H-Al-MFI the energy level changed periodically indicating the strong vibration of the framework. On the other hand the change in energy level for H-Al-BEA was very small, which meant the thermally stable framework of BEA structure. Fig. 9 and Fig. 10 show the change of bonded interaction energy and cell volume for H-Al-MFI and H-Al-BEA, respectively. The changes of these parameters for H-Al-MFI were much larger, indicating that H-Al-MFI has a high strain in the structure. In such an unstable state, namely at a high bonded interaction energy level, the framework structure was highly distorted as shown in Fig. 11. The unit cell expanded as the energy level decreased. This meant that the bond interactions tended to break and would result in the collapse

Table 2
Amount and average potential energy of ammonia adsorbed on various metallosilicates simulated by computer

		Monometallo			Bimetallo		
		Al	Ga	Fe	Al, Ga	Al, Fe	Ga, Fe
Amount of NH_3 (g/mol metal)	MFI	30.6	21.7	4.34	30.5	20.9	14.2
	BEA	19.9	14.4	2.40	17.5	11.2	8.00
Potential energy (kcal/mol NH_3)	MFI	−7.66	−6.72	−3.26	−7.31	−7.17	−6.31
	BEA	−8.06	−6.42	−2.72	−7.46	−57.32	−5.64

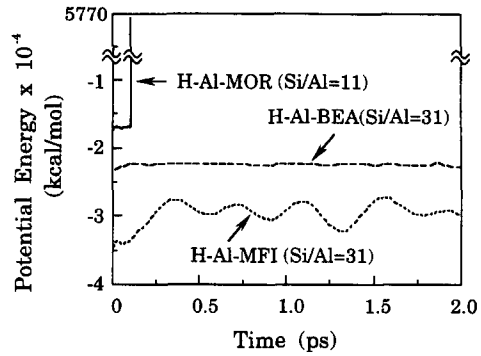

Fig. 8. Change in potential energy of H-Al-MFI, H-Al-BEA, and H-Al-MOR at 1300 K with a function of time.

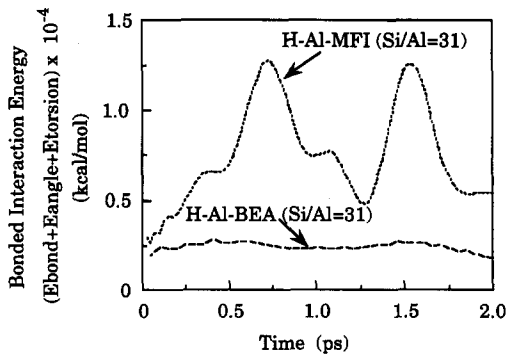

Fig. 9. Change in bonded interaction energy of H-Al-MFI and H-Al-BEA at 1300 K with a function of time.

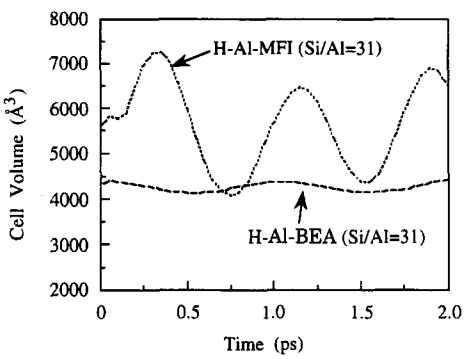

Fig. 10. Change in cell volume of H-Al-MFI and H-Al-BEA at 1300 K with a function of time.

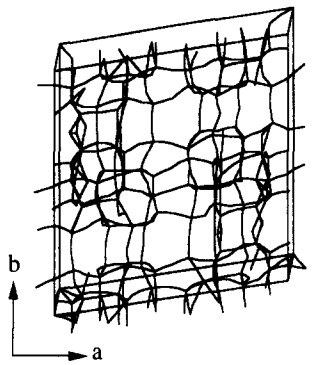

Fig. 11. Framework of H-Al-MFI depicted by computer simulation with the temperature condition at 1300 K.

of the whole structure. This kind of information hardly obtained from experimental results and methods can be a strong tool for developing novel highly designed catalysts which are used in severe conditions like diesel engine exhaust purifications.

4. Conclusion

Active catalytic metal-species incorporated into the framework or involved in the zeolite matrix with a crystallographic regularity were dispersed much higher than those supported by the ion-exchange method or the incipient impregnation method. Nevertheless, the former were more stable against the repeating redox treatments and could take the medium oxidation state of metals, which is significant for the NO decomposition. Solid acidity with proper strength contained in zeolite and metallosilicate catalysts enhances decomposition and conversion of hydrocarbon added and supply to the oxidized catalyst surface. Combustion of hydrocarbon molecules on the oxidized catalyst surface affords reduced spots, where decomposition reaction of NO could advance. Computer simulation supported existence of localized active sites and the evaluation of thermal strength of different types of zeolites.

Acknowledgements

This work was partly supported by a Grants-in-Aids for Development Scientific Research [(A) (2) No. 06505005] from the Ministry of Education, Science and Culture of Japan.

References

[1] H. Hamada, Y. Kintaichi, M. Sasaki and T, Ito, Appl. Catal., 64 (1990) L1.
[2] M. Sasaki, H. Hamada, Y. Kintaichi and T. Ito, Catal. Lett., 15 (1992) 297.
[3] H. Hamada, Y. Kintaichi, M. Sasaki and T. Ito, Appl. Catal., 75 (1991) L1.
[4] H. Hamada, Y. Kintaichi, M. Tabata, M. Sasaki and T. Ito, Chem. Lett., (1991) 2179.
[5] M. Iwamoto, H. Yahiro, S. Shundo, Y. Yu-u and N. Mizuno, Shokubai (Catalyst), 32 (1990) 430.
[6] S. Sato, Y. Yu-u, H. Yahiro, N. Mizuno and M. Iwamoto, Appl. Catal., 70 (1990) L1.
[7] M. Misono and K. Kondo, Chem. Lett., (1991) 1001.
[8] K. Yogo, M. Ihara, I. Terasaki and E. Kikuchi, Chem. Lett., (1993) 229.
[9] Y. Li and J.M. Armor, Appl. Catal. B, 1 (1992) L31.
[10] H. Hamada, Y. Kintaichi, M. Tabata, M. Sasaki and T. Ito, J. Jpn. Petrol. Inst., 36 (1993) 149.
[11] M. Iwamoto, H. Yahiro and N. Mizuno, in R. von Ballmoos, J.B. Higgins and M.M.J. Treacy (Editors), Proc. 9th Intern. Zeolite Confer., Montreal, July 5–10, 1992, Butterworth-Heinemann, Stoneham, 1993, p. 397.
[12] T. Nakatsuji, H. Shimizu and R. Yasukawa, Shokubai (Catalyst), 36 (1994) 100.
[13] T. Inui, O. Yamase, K. Fukuda, A. Ito, J. Tarumoto, N. Morinaga, T. Hagiwara and Y. Takegami, in Proc. 8th Intern. Congr. Catal., Berlin, 1984, Dechema, Frankfurt-am-Main, 1984, Vol. 3, p. 569.
[14] T. Inui, ACS Symp. Series, 398 (1989) 379.
[15] T. Inui, Y. Makino, F. Okazumi, S. Nagano and A. Miyamoto, I and EC. Res., 26 (1987) 647.
[16] T. Inui, H. Nagata, F. Okazumi and H. Matsuda, Catal. Lett., 13 (1992) 297.
[17] T. Inui, Pet. Technol., 16 (1993) 421.
[18] T. Inui, S. Phatanasri and H. Matsuda, J. Chem. Soc., Chem. Commun., 112 (1990) 10.
[19] T. Inui, S. Iwamoto and S. Shimizu, in R. von Ballmoos, J.B. Higgins and M.M.J. Treacy (Editors), Proc. 9th Intern. Zeolite Confer., Montreal, July 5–10, 1992, Butterworth-Heinemann, Stoneham, 1993, p. 405.
[20] T. Inui, T. Hirabayashi, S. Iwamoto and S. Shimizu, Catal. Lett., 27 (1994) 267.
[21] A.K. Rappe and W.A. Goddard III, J. Phys. Chem., 95 (1991) 3358.
[22] S. Dasgupta and W.A. Goddard III, J. Phys. Chem., 90 (1989) 7217.
[23] M.R. Stapleton, D.J. Tildesley and N. Quirke, J. Chem. Phys., 92 (1992) 4456.
[24] T. Inui, in Proc. Int. Conf. on Zeolite Catalysis for the Solution of Environmental Problems, Yaroslavl, Russia, 1992, in press.
[25] M. Iwamoto, H. Yahiro, Y. Mine and S. Kagawa, Chem. Lett., (1989) 213.

[26] M. Iwamoto, H. Yahiro, Y. Mine, Y. Furukawa and S. Kagawa, Shokubai (Catalyst), 31 (1989) 385.
[27] T. Inui, S. Kojo, M. Shibata, T. Yoshida and S. Iwamoto, in Studies in Surface Science and Catalysis, Vol. 69, Elsevier, Amsterdam, 1991, p. 355.
[28] T. Inui, J. Jpn. Petrol. Inst., 33 (1990) 198.
[29] T. Inui, H. Wakita and H. Fukuzawa, MSR Intern. Meeting on Adv. Mats., Vol. 2, 1989, p. 189.
[30] T. Inui, T. Ueda, M. Suehiro and H. Shingu, J. Chem. Soc., Faraday Trans, 1, 74 (1978) 2490.
[31] T. Inui, T. Ueda, M. Suehiro and H. Shingu, J. Jpn. Chem. Soc., (1976) 1665.
[32] T. Inui, T. Ueda and M. Suehiro, J. Jpn. Chem. Soc., (1977) 934.
[33] T. Inui and T. Iwana, Catalysis on the Energy Scene in Studies in Surface Science and Catalysis, Vol. 19, Elsevier, Amsterdam, 1984, p. 205.
[34] S. Tanabe and M. Matsumoto, Chem. Lett., (1985) 1425.
[35] T. Inui, Y. Adachi, T. Kuroda, M. Hanya and A. Miyamoto, Chem. Express, 1 (1986) 255.
[36] T. Inui, S. Iwamoto, S. Kojo, S. Shimizu and T. Hirabayashi, Catal. Today, 22 (1994) 41.
[37] T. Inui and S. Kojo, unpublished data.
[38] T. Inui and K. Matsuba, Stud. Surf. Sci. Catal., 90 (1994) 355.
[39] T. Inui and J. Ito, J. Jpn. Petrol. Inst., 36 (1993) 114.
[40] K. Matsuba, Y. Tanaka, N. Goto, Y. Nakazaki and T. Inui, Preprints, 65th Annual Meeting of Chem. Soc. Japan, I (1993) 436.